Analysis of Thermal Radiation and Ohmic Heating Effects on the Entropy Generation of MHD Williamson Fluid through an Inclined Channel

4 authors, including:

Abiodun Opanuga
Covenant University Ota Ogun State, Nigeria
116 PUBLICATIONS   **1,257** CITATIONS

SEE PROFILE

Gbeminiyi Sobamowo
University of Lagos
346 PUBLICATIONS   **1,642** CITATIONS

SEE PROFILE

Hilary Okagbue
Covenant University Ota Ogun State, Nigeria
256 PUBLICATIONS   **2,541** CITATIONS

SEE PROFILE

Analysis of Thermal Radiation and Ohmic Heating Effects on the Entropy Generation of MHD Williamson Fluid through an Inclined Channel

ABIODUN OPANUGA[1], GBEMINIYI SOBAMOWO[2], HILARY OKAGBUE[1],
PETER OGUNNIYI[1]
[1]Department of Mathematics, Covenant University, Ota, NIGERIA
[2]Department of Mechanical Engineering, University of Lagos, Akoka, Lagos, NIGERIA

Abstract: -In this present work, the heat irreversibility analysis of thermal radiation, Ohmic heating, and angle of inclination on Williamson fluid is presented. The developed equations are converted to dimensionless forms, and Homotopy perturbation method (HPM) is used to solve the resulting coupled ordinary differential equations. The heat irreversibility analysis is achieved by substituting the obtained results into entropy generation and Bejan number expressions. The HPM solution for the velocity profile is validated by comparing it with a previously published study in some limited cases, and an excellent agreement is established. Fluid motion is accelerated by the increasing values of thermal radiation parameter, whereas the magnetic parameter and Reynolds number reduce it. Furthermore, except for the Weissenberg and Prandtl numbers, all of the flow parameters examined enhance fluid temperature. In addition, entropy generation is enhanced at the channel's upper wall for all parameters except magnetic field parameter.

Key-Words: -Williamson fluid, heat irreversibility, thermal radiation, inclined channel, Homotopy perturbation method.

1 Introduction

Many researchers have been fascinated by the study of viscous incompressible non-Newtonian fluids in recent decades because of their wide applications in engineering and industry. Non-Newtonian fluids do not follow Newton's law of viscosity (the shear stress to shear rate ratio is always the same). Since the Navier-Stokes equations alone are insufficient to represent the rheological features of these fluids, therefore to address this flaw, several rheological models have been proposed, including the Ellis, Power-law, Carreaus, Cross, and pseudoplastic fluids. Pseudoplastic fluids are more significant among these because of their extensive applications in industries such as melting of high molecular weight polymers, photographic films, and polymer sheet extrusion. Williamson, [1], investigated the flow of pseudoplastic materials and developed a model to characterize their behaviour, and further explained that the fluid captures the thinning properties of non-Newtonian fluids. Thereafter, several investigators have been involved in the analysis of this fluid. Khan and Alzahrani, [2], discovered that the Weissenberg number (We) has an inverse relationship with velocity. However, it is enhanced as the mixed convection parameter increases. The stretching sheet Williamson flow was studied by Nadeem et al., [3]. As demonstrated by Hayat et al., [4], magnetic and electric fields, as well as thermal radiation, have an effect on the flow pattern of a two-dimensional flow of Williamson fluid with porosity. Krishnamurthy et al., [5], investigated a steady flow of Williamson fluid in a horizontal linearly stretched sheet with simultaneous chemical reaction, melting heat transfer, and nanoparticles. Dapra and Scarpi,[6],presented the perturbation solution for pulsatile motion of Williamson fluid. In view of the significance of peristaltic motion of the non-Newtonian fluid through asymmetric channels along porous walls, Vajravelu et al., [7], explored this using varied phase and amplitude, as well as the manipulation of different wave patterns on the fluid flow model. Raza et al., [8], examined hydromagnetic Williamson nanofluid with slip conditions. It was submitted that Williamson fluid parameter and the temperature profile had a direct relationship. Vasudev et al., [9], investigated the peristaltic Williamson fluid in a planar channel, and the flow was explored in a wave framework that flowed with the speed of the wave. Nadeem et al., [10], proposed a model for the motion of Williamson fluid in an annular zone. Using the Keller box approach, Malik et al., [11], studied the Williamson fluid model

across a stretched cylinder Vittal et al., [12],reported hydromagnetic stagnation point Williamson fluid flow on exponential stretchable surface. Monica et al., [13], proposed an analysis for non-Newtonian fluids stagnation point flow through a stretching sheet. The modelling of two-dimensional Williamson fluids through a circular cylinder was presented by Nagaraja and Reddy, [14]. Using the Adomian decomposition method, Siddiqui et al., [15], discovered an analytical approach of Williamson fluid Blade coating analysis. Shashikumar et al., [16], analysed the steady flow of Williamson fluid in a micro-channel caused by viscous dissipation, magnetic effect, and Joule dissipation. For further details on flow accounting for the viscoelastic shear thinning characteristics of non-Newtonian fluids, interested readers can consult the extensive research in [17-18].

Ohmic heating is a type of heating technique in which electrical current is used to generate heat in fluid materials. It is produced by the applied electric field and fluid electrical resistance, which is the conversion of electric energy to thermal energy. Numerous researchers have investigated Newtonian and non-Newtonian fluid flow problems in the context of Ohmic heating and heat transfer. The viscosity effect on the Joule heating rate of solid-liquid mixtures was investigated by Khalaf and Sastry, [19]. It was submitted that fluid mixture with higher viscosity has higher rate of heating than the mixture with lower viscosity fluid. The study of hydromagnetic heat transfer and boundary layer flow with Ohmic heating and chemical reaction was conducted by Rao et al., [20]. It was submitted that increasing values of Joule heating parameter improves temperature and concentration distributions of nanofluid. Prakash et al., [21], investigated an electrically conducting nanofluid's mixed convective flow in a porous medium: the effects of a variable magnetic field. Tsai et al., [22],studied the effects of Ohmic heating and heat transfer on electrically conducting flow with variable viscosity. Awasthi, [23], analysed the significance of Ohmic heating and thermal radiation effects on MHD convective flow using perturbation technique. Furthermore, Muhammad et al., [24], presented an analyses on chemical reaction and viscous dissipation influence on electrically conducting flow of Newtonian fluid past an exponentially stretching sheet with the Ohmic heating. Adegbie et al., [25], conducted an analysis on free convection flow over a moving porous surface under the influence of Joule heating and magnetic field. Osalusi et al., [26], considered Joule heating and viscous dissipation effects on transient hydromagnetic and slip flow over a permeable rotating disk.

Ohmic heating effect on non-Newtonian fluids has also been investigated by several researchers. Goud and Nandeppanavar, [27], conducted a study on Ohmic heating and chemical reaction effects on hydromagnetic flow of micropolar fluid. Hasan et al., [28], considered Peristaltic wave-induced Hall current and Ohmic heating in a non-Newtonian channel flow. Gireesha et al., [29],investigated the influence of Joule heating on Casson fluid hydromagnetic mixed convection flow by taking cross diffusion into account. Samuel and Olajuwon, [30],studied theeffects of thermal radiation,Joule heating on Maxwell fluid with Lorentz and buoyancy forces.

Irreversibility analysis in gravity-driven flows has applications in nature, for example, in the printing field, during paper manufacturing processes, wire drawing, spaying,fibreglass in metallurgical technology. Bejan,[31,32], applied the second law of thermodynamics to aid the understanding of fluid entropy generation rate and minimization of irreversibilities processes. Furthermore, Bejan, [33, 34], analysed the volumetric entropy generation rate in fluid flow processes, and this has been adopted by several scholars. To provide a brief overview of the application of the second law analysis approach to monitoring entropy buildup on inclined walls. The flow of a Newtonian film along a heated inclined plate has been reportedby Saouli and Aboud-Saouli, [35], with the goal of increasing the available energy for work. The notion of a variable viscosity fluid flowing down the channel was developed by Havzali et al., [36]. Tshela, [37], used aspect ratio approximations in the lubrication theory for a temperature-dependent viscous flow in the boundary layer with Newtonian heating. Furthermore, Al-Ahmed et al., [38],studied energy reduction in free and constrained gravity-driven film flows of varied viscosity through heated plates.The steady, reactive flow of a couple stress fluid through a porous medium was studied by Adesanya et al., [39]. Adesanya and Makinde, [40], used the Adomian decomposition method to investigate entropy generation of third-grade fluid flow along a vertical channel and the impact of internal heat generation. See Refs [41-46] for further reading.

He [47] proposed the Homotopy Perturbation Method (HPM), which is a combination of topology's homotopy and traditional perturbation techniques. This enables us to obtain analytic or approximate solutions tonumerous problems occurring in a number of scientific fields. The

technique demonstrates rapid convergence of the series solution and provides a wide range of benefits. It also offers an analytical approximate solution for non-linear equations in the form of an infinite series, from which each term can be deduced one by one. In recent years, researchers have concentrated their efforts on solving both linear and nonlinear ordinary and partial differential equations. The approach has successfully handled several types of linear and nonlinear differential equationsincluding the Lighthill equation [48], Duffing equation [49], Blasius equation [50], wave equations [51], and boundary value problems [52]. Numerous authors have lately conducted extensive research on the homotopy perturbation technique and used it to tackle nonlinear problems. This approach has been improved [53–56] to provide more accurate results, help accelerate the series solution's rapid convergence, and minimize the computational effort.

In light of the present literature survey, it is obvious that entropy generation in Williamson fluid in the presence of Rosseland thermal radiation and Joule heating in an inclined channel has not been accorded the required attention in view of the important applications of flow powered by gravitational force in many food industries, polymerization operations, heat exchangers, film evaporators,wire and glass production, and drying processes. In addition, the outcome of this investigation can support research work on emulsion coated sheets like photographic films and blood flow. Consequently, this current study's goal is to apply the energy evaluation technique as a useful tool for identifying variables related to the loss of available energy for work and as a measure of thermal equipment efficiency in order to reduce waste. Furthermore, the HPM approach applied in this study is presented in a more appealing and systematic manner. The technique is easy to apply because it does not require discretization, transformation, formulation of Adomian and homotopy polynomials.

2 Problem Formulation

A fully developed steady and incompressible hydromagnetic laminar flow of Williamson fluid is considered as depicted in Figure 1. The fluid is flowing between two infinite parallel plates with distance h apart, inclined at an angle γ. The Cartesian coordinates system approach is such that the flow is along $x-axis$ direction while the $y-axis$ is perpendicular to the flow. A magnetic

field of strength B_0 is applied transversely to the flow. It is assumed that the physical quantities depend on y only and the magnetic Reynolds number is considered to be low, resulting in a negligible induced magnetic field in comparison to the applied magnetic field. It is furthermore assumed that the imparted electric field is zero, and that the Hall effect is disregarded. The fluid motion is given by the following set of equations using Boussinesq's approximation.
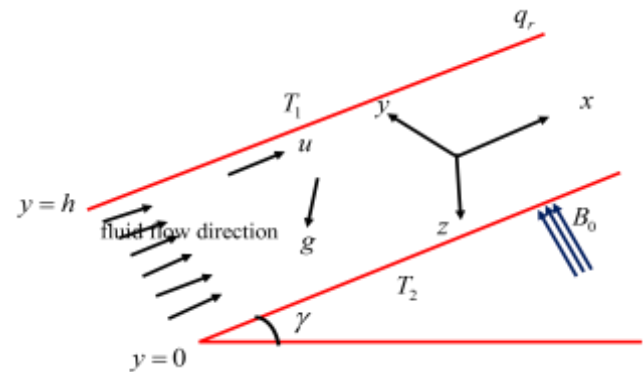

Fig. 1: Schematic Diagram of the Problem

For an electrically conducting fluid, the Ohm's law when Hall currents, ion-slip and thermoelectric effects, as well as the electron pressure gradient are ignored is:

$$\mathbf{J} = \sigma\left[\mathbf{E} + \mathbf{q} \times \mathbf{B}\right] \qquad (1)$$

where $\mathbf{E}$ denotes the electric field vector, $\mathbf{J}$ is the current density vector, $\mathbf{q}$ is the velocity vector, and σ represents the fluid's electrical conductivity and $\mathbf{B}$ is the magnetic field vector. The total magnetic field $\mathbf{B}\left(=\mathbf{B}_0 + \mathbf{b}\right)$. The applied and induced magnetic fields are denoted by $\mathbf{B}_0$ and $\mathbf{b}$, respectively. The induced magnetic field is not taken into account for small magnetic Reynolds numbers.

Following the aforementioned assumptions, the momentum and energy equations take the form [16]

$$\rho v_0 \frac{du}{dy} = -\frac{dp}{dx} + \mu\left(1 + \sqrt{2}\Gamma \frac{du}{dy}\right)\frac{d^2u}{dy^2} + \rho g\left(T - T_1\right)\sin\left(\gamma\right) + B_0 J_z \qquad (2)$$

$$\rho c_p v_0 \frac{dT}{dy} = k\frac{d^2T}{dy^2} + \mu\left(1+\frac{\Gamma}{\sqrt{2}}\frac{du}{dy}\right)\left(\frac{du}{dy}\right)^2 \tag{3}$$
$$-\frac{dq_r}{dy} + \lambda\frac{J^2}{\sigma}$$

The index λ is set at 1 for the inclusion of Joule dissipation. Taking

$$\mathbf{E}_x = 0, \mathbf{E}_z = 0, \Rightarrow \mathbf{J}_x = 0, \mathbf{J}_x = -\sigma B_0 u \tag{4}$$

Equations (2) and (3) are transformed by the use of (4)

$$\rho v_0 \frac{du}{dy} = -\frac{dp}{dx} + \mu\left(1+\sqrt{2}\Gamma\frac{du}{dy}\right)\frac{d^2u}{dy^2} - \sigma B_0^2 u + \tag{5}$$
$$\rho g (T-T_1)\sin(\gamma)$$

$$\rho c_p v_0 \frac{dT}{dy} = k\frac{d^2T}{dy^2} + \mu\left(1+\frac{\Gamma}{\sqrt{2}}\frac{du}{dy}\right)\left(\frac{du}{dy}\right)^2 + \tag{6}$$
$$\sigma B_0^2 u^2 - \frac{dq_r}{dy}$$

The boundary conditions are as follows:
$$u(0)=0, u(h)=0, T(0)=T_2, T(h)=T_1 \tag{7}$$

The net radiative heat flux q_r for optically thick material is obtained using the Rosseland approximation.

$$q_r = -\frac{4\sigma^c}{3k^c}\frac{\partial T^4}{\partial y} \tag{8}$$

T^4 is being expanded in a Taylor series about T_0 as.
$$T'^4 \cong T_0^4 + 4T_0^3(T-T_0) + 6T_0^2(T-T_0)^2 + \tag{9}$$
$$4T_0(T-T_0)^3 + \ldots$$

and ignoring the higher order components, yields
$$T'^4 \cong 4T_0^3 T - 3T_0^3 \tag{10}$$

In light of equations (4) and (6), equation (3) yields
$$\rho c_p v_0 \frac{dT}{dy} = k\frac{d^2T}{dy^2} + \mu\left(1+\frac{\Gamma}{\sqrt{2}}\frac{du}{dy}\right)\left(\frac{du}{dy}\right)^2 + \tag{11}$$
$$\sigma B_0^2 u^2 + \frac{16\sigma^c T^3}{3k^c}\frac{d^2T}{dy^2}$$

To obtain similarity equations, the following similarity transformations are utilized.

$$u = \frac{\mu}{\rho h}f(\eta), \eta = \frac{y}{h}, \theta(\eta) = \frac{T-T_1}{T_2-T_1} \tag{12}$$

which yield
$$\left(1+Wef'(\eta)\right)f''(\eta) - \mathrm{Re}\,f'(\eta) - M^2 f(\eta) + \tag{13}$$
$$Gr\theta\sin(\gamma) + A = 0$$

$$\left(1+\frac{4}{3}Ra\right)\theta''(\eta) - \mathrm{Re}\,\mathrm{Pr}\,\theta'(\eta) +$$
$$Ec\,\mathrm{Pr}\left(1+\frac{We}{2}f'(\eta)\right)\left(f'(\eta)\right)^2 + \tag{14}$$
$$M^2 f^2(\eta) = 0$$

with the relevant boundary conditions given as
$$f(0)=0, f(1)=0, \theta(0)=1, \theta(1)=0 \tag{15}$$

where
$$\mathrm{Re} = \frac{\rho v_0 h}{\mu}, A = \frac{\rho h^3}{\mu^2}\left(-\frac{dp}{dx}\right), We = \frac{\sqrt{2}\mu\Gamma}{\rho h^2},$$
$$M^2 = \frac{\sigma B_0^2 h^2}{\mu}, Gr = \frac{\rho^2 h^3 g\beta(T_2-T_1)}{\mu^2}, \tag{16}$$
$$Ra = \frac{4\sigma^c T_\infty^3}{k^c k}$$

3 Analysis of Homotopy Perturbation Method(HPM)

Given a nonlinear differential equation

$$\lambda(u) - f(r) = 0, r \in \Omega, \tag{17}$$

And the boundary conditions expressed as

$$\psi\left(u, \frac{\partial u}{\partial \eta}\right) = 0, r \in \Gamma, \tag{18}$$

Where λ is a general differential operator, ψ is a boundary operator, $f(r)$ is a known analytical function, and Γ is the boundary of the domain Ω. The operator λ is written as linear operator, L and nonlinear operator N. Then, equation(1)can be expressed as:

$$L(u) + N(u) - f(r) = 0, r \in \Omega. \tag{19}$$

Using He's Homotopy technique to construct a homotopy $\upsilon(r,p):\Omega\times[0,1]\to R$, and this satisfies

$$H(\upsilon,p)=(1-p)\big[L(\upsilon)-L(u_0)\big]+$$
$$p\big[\lambda(\upsilon)-f(r)\big]=0 \tag{20}$$

or

$$H(\upsilon,p)=L(\upsilon)-L(u_0)+$$
$$p\big[L(u_0)+N(\upsilon)-f(r)\big]=0, \tag{21}$$

where $p\in[0,1]$ is an embedding parameter, u_0 is an initial approximation of Eqn. (1).

It is obvious that equations (20) and (21) yield

$$H(\upsilon,0)=L(\upsilon)-L(u_0)=0,$$

$$H(\upsilon,1)=\lambda(\upsilon)-f(r)=0,$$

As p varies from zero to unity, $\upsilon(r,p)$ from $u_0(r)$ to $u(r)$. In topology, this is regarded to as homotopy. The embedding parameter p can be utilized by HPM as a small parameter and assuming that the solutions of equations (20) and (21) can be written as a power series in p.

$$\upsilon=p^0\upsilon_0+p^1\upsilon_1+p^2\upsilon_2+p^3\upsilon_3+\cdots. \tag{22}$$

Setting $p=1$, yields the approximate solution of equation (17)

$$\upsilon=\lim_{p\to1}=\upsilon_0+\upsilon_1+\upsilon_2+\upsilon_3+\cdots. \tag{23}$$

4 Method of Solution by HPM

Homotopy perturbation method is used to solve the dimensionless nonlinear Equations (13)-(14). As a result, a homotopy construction for Equations (13)-(14) is developed for the current problem:

$$H(f,p)=(1-p)f''(\eta)+$$
$$p\begin{bmatrix}f''(\eta)+Wef'(\eta)f''(\eta)-\mathrm{Re}\,f'(\eta)-\\M^2f(\eta)+Gr\theta\sin(\gamma)+A\end{bmatrix} \tag{24}$$

and

$$H(f,p)=(1-p)\left(1+\frac{4}{3}Ra\right)\theta''(\eta)+$$
$$p\begin{bmatrix}\left(1+\frac{4}{3}Ra\right)\theta''(\eta)-\mathrm{Re}\,\mathrm{Pr}\,\theta'(\eta)+\\Ec\,\mathrm{Pr}\left(1+\frac{We}{2}f'(\eta)\right)f''(\eta)+M^2f'(\eta)\end{bmatrix} \tag{25}$$

and $p[0,1]$ is an embedding parameter, then for $p=0$ and $p=1$

$$f(\eta,0)=f_0(\eta),f(\eta,1)=f_1(\eta);$$
$$\theta(\eta,0)=\theta_0(\eta),\theta(\eta,1)=\theta_1(\eta) \tag{26}$$

It is noteworthy that as p rises from zero to one, $f(\eta,p)$ shifts from $f_0(\eta)$ to $f_1(\eta)$ and $\theta(\eta,0)$ shifts from $\theta_0(\eta)$ to $\theta_1(\eta)$. Assume that the solution to Equations (13)-(14) is represented as a p-series:

$$f(\eta)=f_0(\eta)+pf_1(\eta)+p^2f_2(\eta)+$$
$$p^3f_3(\eta)+\cdots=\sum_{i=0}^{n}p^if_i(\eta) \tag{27}$$

and

$$\theta(\eta)=\theta_0(\eta)+p\theta_1(\eta)+p^2\theta_2(\eta)+$$
$$p^3\theta_3(\eta)+\cdots=\sum_{i=0}^{n}p^i\theta_i(\eta) \tag{28}$$

After substituting Equations (27) and (28) into Equations (13) and (14) respectively, the subsequent expression will appear in the form of a polynomial in p and expanding such that terms of the same order of p are categorized together. Furthermore, a set of differential equations is derived together with their associated boundary conditions by setting the polynomial coefficients in p to one, yields

$$p^0 : f_0''(\eta) + A = 0; f_0(0) = 0, f_0(1) = 0,$$
$$p^1 : f_1''(\eta) + We(f_0'f_0'') - \operatorname{Re} f_0' - M^2 f_0 +$$
$$Gr\theta_0 \sin(\gamma); f_1(0) = 0, f_1(1) = 0,$$
$$p^2 : f_2''(\eta) + We(f_0'f_1'' + f_1'f_0'') - \operatorname{Re} f_1' -$$
$$M^2 f_1 + Gr\theta_1 \sin(\gamma); f_2(0) = 0, f_2(1) = 0, \quad (29)$$
$$p^3 : f_3''(\eta) + We(f_0'f_2'' + f_2'f_0'' + f_1'f_1'') -$$
$$\operatorname{Re} f_2' - M^2 f_2 + Gr\theta_2 \sin(\gamma);$$
$$f_3(0) = 0, f_3(1) = 0$$

And

$$p^0 : \left(1 + \frac{4}{3} Ra\right)\theta_0'' = 0, \theta_0(0) = 1; \theta_0(1) = 0,$$

$$p^1 : \left(1 + \frac{4}{3} Ra\right)\theta_1'' - \operatorname{Re}\operatorname{Pr}\theta_0' + Ec\operatorname{Pr}(f_0')^2 +$$

$$Ec\operatorname{Pr}\frac{We}{2}(f_0')^3 + M^2(f_0)^2 = 0; \theta_1(0) = 0,$$

$$\theta_1(1) = 0,$$

$$p^2 : \left(1 + \frac{4}{3} Ra\right)\theta_2'' - \operatorname{Re}\operatorname{Pr}\theta_1' +$$

$$Ec\operatorname{Pr}(2f_0'f_1') + Ec\operatorname{Pr}\frac{We}{2}(3f_0'f_0'f_1') +$$

$$M^2(2f_0f_1) = 0; \theta_2(0) = 0, \theta_2(1) = 0$$

$$p^3 : \left(1 + \frac{4}{3} Ra\right)\theta_3'' - \operatorname{Re}\operatorname{Pr}\theta_2' +$$

$$Ec\operatorname{Pr}\left(2f_0'f_2' + (f_1')^2\right) +$$

$$Ec\operatorname{Pr}\frac{We}{2}\left(3f_0'f_0'f_2' + 3f_0'f_1'f_1'\right) +$$

$$M^2\left(2f_0f_2 + (f_1)^2\right) = 0; \theta_3(0) = 0, \theta_3(1) = 0. \quad (30)$$

The following results are obtained upon solving Equations (29)–(30).

$$f_0(\eta) = \frac{1}{2}(A\eta - A\eta^2), \quad (31)$$

$$f_1(\eta) =$$
$$\frac{1}{24}\begin{pmatrix} -AM^2\eta - 2A\operatorname{Re}\eta - 2A^2We\eta + \\ 6A\operatorname{Re}\eta^2 + 6A^2We\eta^2 + 2AM^2\eta^2 \\ -4A\operatorname{Re}^3 - 4A^2We\eta^3 - AM^2\eta^4 \\ +8Gr\sin(\gamma)\eta - 12Gr\sin(\gamma)\eta^2 \\ +4Gr\sin(\gamma)\eta^3 \end{pmatrix} \quad (32)$$

$$\theta_0(\eta) = 1 - \eta, \quad (33)$$

$$\theta_1(\eta) = \frac{1}{160(3 + 4Ra)}$$

$$\begin{pmatrix} 2A^2M^2\eta + 20A^2Ec\operatorname{Pr}\eta + \\ 240\operatorname{Pr}\operatorname{Re}\eta + 3A^2Ec\operatorname{Pr}We\eta - \\ 60A^2Ec\operatorname{Pr}\eta^2 - 240\operatorname{Pr}\operatorname{Re}\eta^2 \\ -15A^3Ec\operatorname{Pr}We\eta^2 + 80A^2Ec\operatorname{Pr}\eta^3 + \\ 30A^3Ec\operatorname{Pr}We\eta^3 - 10A^2M^2\eta^4 - \\ 40A^2Ec\operatorname{Pr}\eta^4 - 30A^3Ec\operatorname{Pr}We\eta^4 + \\ 12A^2M^2\eta^5 + 12A^3Ec\operatorname{Pr}We\eta^5 - \\ 4A^2M^2\eta^5 \end{pmatrix} \quad (34)$$

The expressions for $f_2(\eta)$ and $\theta_2(\eta)$ are obtained in the same way. These expressions, however, not included in this write-up. The HPM solutions of Equations (24) and (25) can be written as:

$$\left.\begin{aligned} f(\eta) &= f_0(\eta) + pf_1(\eta) + p^2 f_2(\eta) + \cdots \\ \theta(\eta) &= \theta_0(\eta) + p\theta_1(\eta) + p^2\theta_2(\eta) + \cdots \end{aligned}\right\} \quad (35)$$

At $p = 1$, the approximate expressions for equations (13) and (14) can be written as

$$\left.\begin{aligned} f(\eta) &= \lim_{p \to 1} f(\eta) = f_0(\eta) + f_1(\eta) + \\ &\quad f_2(\eta) + \cdots \\ \theta(\eta) &= \lim_{p \to 1} \theta(\eta) = \theta_0(\eta) + \theta_1(\eta) + \\ &\quad \theta_2(\eta) + \cdots \end{aligned}\right\} \quad (36)$$

Substituting Equations (31)-(34) into Equation (36), yields

$$f(\eta) = \frac{1}{2}(A\eta - A\eta^2) -$$

$$\frac{1}{24}\begin{pmatrix} -AM^2\eta - 2A\,\mathrm{Re}\,\eta - \\ 2A^2We\eta + 6A\,\mathrm{Re}\,\eta^2 + \\ 6A^2We\eta^2 + 2AM^2\eta^3 - \\ 4A\,\mathrm{Re}\,\eta^3 - 4A^2We\eta^3 - \\ AM^2\eta^4 - AM^2\eta^4 + \cdots \end{pmatrix} \quad (37)$$

and

$$\theta(\eta) = 1 - \eta + \frac{1}{160(3+4Ra)}$$

$$\begin{pmatrix} 2A^2M^2\eta + 20A^2Ec\,\mathrm{Pr}\,\eta + \\ 240\,\mathrm{Pr}\,\mathrm{Re}\,\eta + 3A^3Ec\,\mathrm{Pr}\,We\eta - \\ 60A^2Ec\,\mathrm{Pr}\,\eta^2 - 240\,\mathrm{Pr}\,\mathrm{Re}\,\eta^2 - \\ 15A^3Ec\,\mathrm{Pr}\,We\eta^2 + 80A^2Ec\,\mathrm{Pr}\,\eta^3 \\ +30A^3Ec\,\mathrm{Pr}\,We\eta^3 + \cdots \end{pmatrix} \quad (38)$$

5 Result Validation

The exact solution of the Newtonian case $(We = 0)$ as considered by Makinde and Eegunjobi,[57],is compared with the HPM solution and presented in Table 1, to validate the Homotopy perturbation method solution used in this work. The exact and HPM solutions are found to be in perfect agreement. The exact solution as obtained by Makinde and Eegunjobi,[57],is

$$f(\eta) = \frac{A\left(1 - \eta + \eta e^{\mathrm{Re}} - e^{\eta\mathrm{Re}}\right)}{\mathrm{Re}\left(e^{\mathrm{Re}} - 1\right)} \quad (39)$$

The momentum Equation (13) at
$\mathrm{Re} = 1, A = 1, We = 0, M = 0, Gr = 0$ reduces to

$$f''(\eta) - f'(\eta) + A = 0, f(0) = 0 \quad (40)$$

The HPM solution of Eqn. (40) is expressed as

$$f(\eta) = \frac{A}{2}(\eta - \eta^2) + \frac{A}{12}(3\eta^2 - 2\eta^3 - \eta) -$$
$$\frac{A}{24}(\eta^2 - 2\eta^3 + \eta^4) + \frac{A}{720}\begin{pmatrix} \eta - 10\eta^3 + \\ 15\eta^4 - 6\eta^5 \end{pmatrix} + \cdots \quad (41)$$

The convergence of the solution is also displayed in Table 2.

Table 1. Comparison of Exact and HPM solutionsof Equations (13) at $\mathrm{Re} = 1, A = 1, We = 0$, $M = 0, Gr = 0$.

η	Exact [57]	RK4 [57]	Current
0.1	0.03879297	0.03879297	0.03879298
0.2	0.07114875	0.07114875	0.07114876
0.3	0.09639032	0.09639032	0.09639033
0.4	0.11376948	0.11376948	0.11376949
0.5	0.12245933	0.12245933	0.12245933
0.6	0.12154600	0.12154600	0.12154601
0.7	0.11001953	0.11001953	0.11001954
0.8	0.08676372	0.08676372	0.08676373
0.9	0.05054498	0.05054498	0.05054499

Table 2. Convergence of HPM result for $A = \mathrm{Re} = M^2 = 1, We = Gr = 0$

k	$-\dfrac{d^2 f_k}{dy^2}$	$-\sum\limits_{k=0}^{n}\dfrac{d^2 f_k}{dy^2}$
0	1.000000000	1.000000000
1	0.500000000	1.500000000
2	0.041666667	1.541666667
3	-0.005555556	1.536111111
4	-0.000090939	1.536020172
5	0.0001361332	1.536156305
6	-0.000012261	1.536144044
7	0.000002121	1.536141923
8	-0.0000000002	1.536142450
9	-0.00000001	1.536142450

5.1 Irreversibility Analysis

The irreversibility rate within the flow is calculated using the obtained temperature and velocity results. The expression for heat irreversibility in the presence of magnetic field and thermal radiation is

$$Eg = \underbrace{\frac{k}{T_1^2}\left(\frac{dT}{dy}\right)^2}_{HTEG} + \underbrace{\frac{16\sigma^c T^3}{3k^c}\left(\frac{dT}{dy}\right)^2}_{TREG} +$$
$$\frac{1}{T_1}\left[\underbrace{\mu\left(1 + \frac{\Gamma}{\sqrt{2}}\frac{du}{dy}\right)\left(\frac{du}{dy}\right)^2}_{FFEG} + \underbrace{\sigma B_0^2 u^2}_{MFEG}\right] \quad (42)$$

Where HTEG = Heat Transfer Entropy Generation, TREG = Thermal Radiation Entropy Generation, FFEG = Fluid Friction Entropy Generation and MFEG = Magnetic Field Entropy Generation.
The non-dimension form of equation (42) is obtained by applying relations (16) to yield

$$Ns = \left(1 + \frac{4}{3}Ra\right)\theta'^2 +$$

$$Ec\Pr L\left[\left(1 + \frac{We}{2}f'\right)(f')^2 + M^2 f^2\right] \quad (43)$$

Denoting

$$N_1 = \left(1 + \frac{4}{3}Ra\right)\theta'^2 \text{ and}$$

$$N_2 = Ec\Pr L\left[\left(1 + \frac{We}{2}f'\right)(f')^2 + M^2 f^2\right] (44)$$

Where $L = \dfrac{T_1}{T_2 - T_1}$ and $Ns = \dfrac{E_g T_1^2 h^2}{k(T_2 - T_1)}$

The Bejan number is then written as

$$Be = \frac{N_1}{N_S} = \frac{1}{1+\Phi}, \Phi = \frac{N_2}{N_1} \quad (45)$$

The distribution ratio of fluid irreversibility is denoted by Φ. From 1 to 0, the Bejan number can have any value. When $Be = 0$, irreversibility of fluid friction dominates entropy generation, when $Be = 1$, irreversibility of heat transfer dominates, and when both enhance entropy generation equally $Be = 0.5$.

6 Results and Discussion

For velocity, temperature, and entropy generation the effects of various physical parameters influencing the flow are analyzed for $0.1 \le We \le 1$, $0.5 \le M \le 1.5$, $0.1 \le Ra \le 4.5$, $0.71 \le \Pr \le 7$, $1.5 \le \mathrm{Re} \le 2.5$ and $\pi/6 \le \gamma \le 7\pi/18$ while $Ec = 0.5$, A and L, on the other hand, are each fixed as 1.
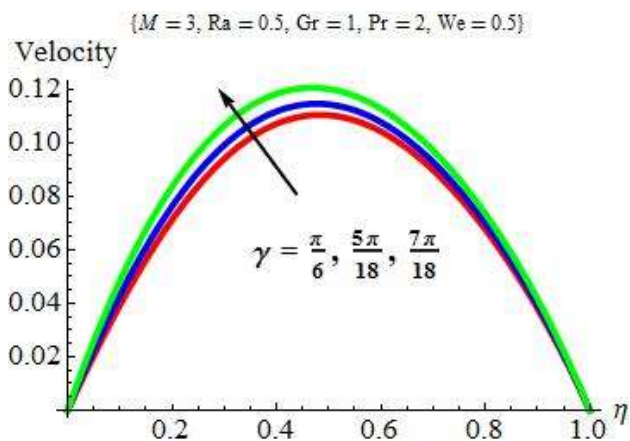
Fig. 2A: γ versus Velocity Profile
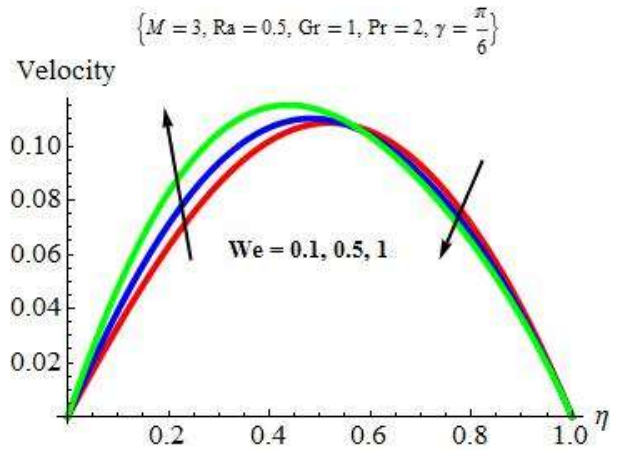
Fig. 2B: We versus Velocity Profile
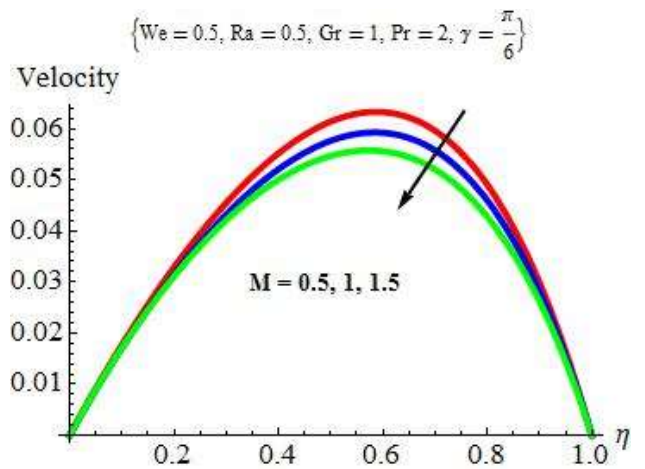
Fig. 2C: M versus Velocity Profile
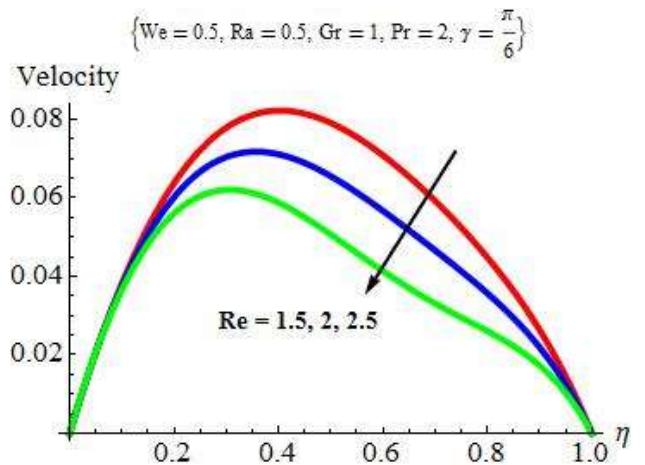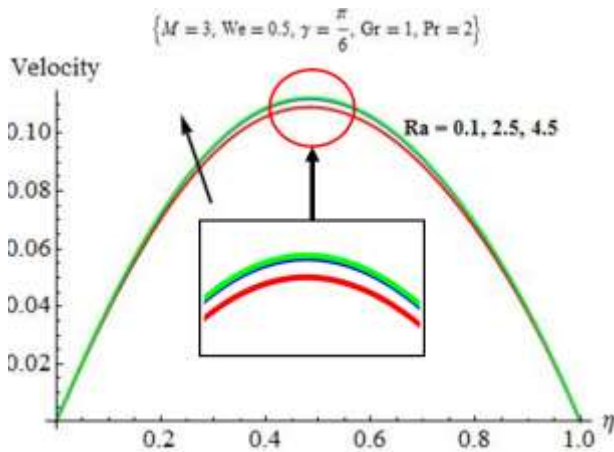

Fig. 2D: Re versus Velocity Profile
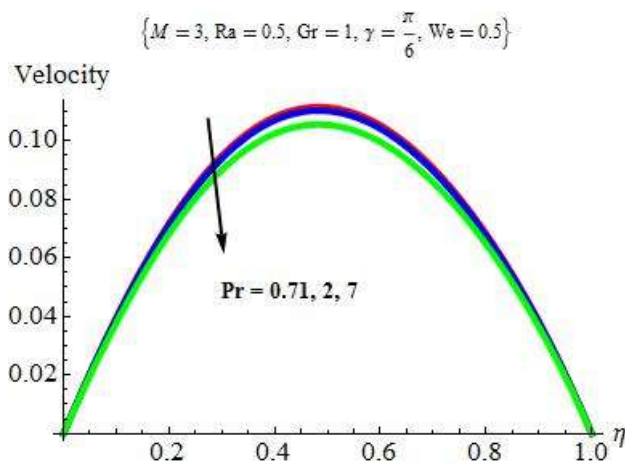
Fig. 2E: Ra versus Velocity Profile

Fig. 2F: Pr versus Velocity Profile

In Figure 2A, the influence of the angle of inclination on fluid velocity is depicted. It is observed that fluid velocity increases as the angle of inclination increases. This observation is due to increased forces acting on the fluid flow. In Figure 2B, the Weissenberg number versus velocity profile is displayed. An increasing trend at the lower wall of the channel is observed while there is a reduction in fluid velocity at the upper wall. Fluid velocity increases with the Weissenberg number (We) at the lower wall due to the shear-thinning effect, while the reduction at the upper wall is due to higher viscosity of the non-Newtonian fluid. The shear-thinning effect is one of the characteristic features of the Williamson fluid. It is a non-Newtonian fluid feature where the fluid's viscosity decreases as the shear stress rises. In addition, the Williamson fluid parameter, measures the effect of viscosity to elasticity. It therefore causes a drop in the velocity profile due to low resistance to flow. In Figure 2C, the response of fluid velocity to the external magnetic field effect is displayed. It is indicated that fluid velocity experiences a reduced momentum. This is to be expected, because the Lorentz force

resulting from the applied magnetic field develops a resistant force within the flow, causing the Williamson fluid motion to reduce. In addition, it is also worth noting that the velocity boundary layer's thickness decreases with a rise in M's value. The velocity response to variations in Reynolds number is displayed in Figure 2D. It is shown that fluid velocity reduces as values of Reynolds number increase. This is physically correct since the Reynolds number signifies the significance of the inertia effect in comparison to the viscous effect. Hence, fluid velocity is retarded as depicted in the figure. An enhancement in fluid velocity with an increase in radiation parameter is observed in Figure 2E, while a falling trend is noticed in Figure 2F for increasing values of Prandtl number. The boundary layer thickness increases, causing more fluid flow and thereby increasing fluid velocity as shown in Figure 2E, while a reverse trend is observed in Figure 2F.
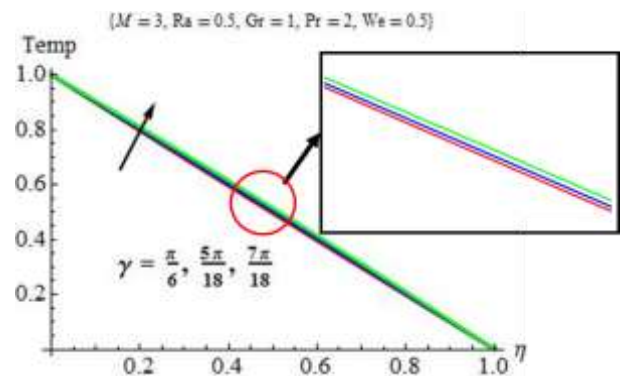

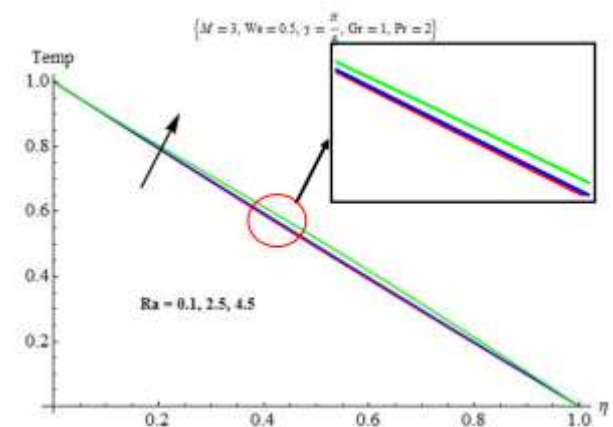Fig. 3A: γ versus Temperature Profile
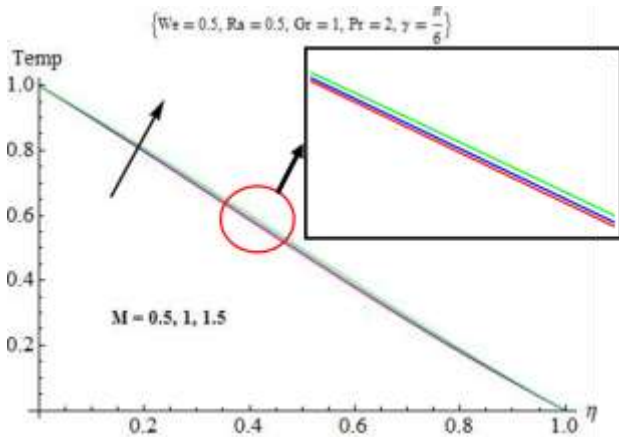

Fig. 3B: Ra versus Temperature Profile
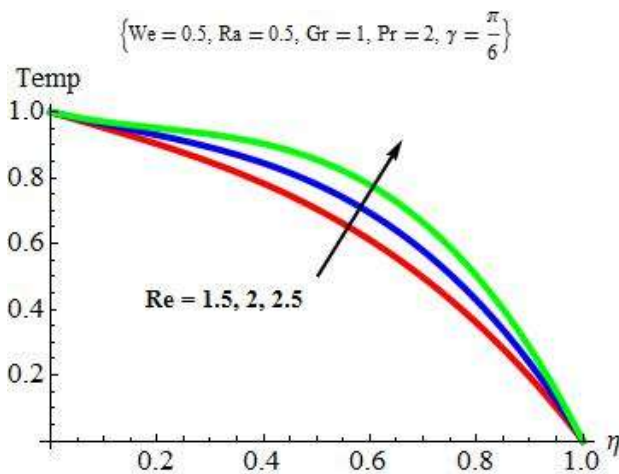
Fig. 3C: M versus Temperature Profile

Fig. 3D: Re versus Temperature Profile

Figure 3 is sketched for various values of inclination angle parameter (γ), Radiation parameter (Ra), magnetic field parameter (M) and Reynolds number (Re). Generally, fluid temperature is enhanced by the rising values of each of the parameters. In Figure 3A, the influence of the angle of inclination parameter is displayed against fluid temperature. As the parameter varies, fluid temperature appears to have risen slightly. This is due to the fact that higher fluid velocity, as shown in Figure 2A, tends to increase the forces acting on fluid flow, resulting in the enhancement of fluid temperature. Figure 3B depicts an increasing trend in fluid temperature with increasing values of radiation parameter.This is attributed to the fact that increasing the radiation parameter $\left(Ra \right)$ decreases the fluid Rosseland absorptivity parameter $\left(k^c \right)$, resulting in an increase in fluid temperature.In Figure 3C, the effect of the magnetic field parameter on fluid temperature is presented. It is observed that as the value of M increases, the temperature rises. Lorentz force is produced when a magnetic field is applied to an electrically conducting fluid and interacts with it.

Because the Lorentz force slows fluid motion, kinetic energy is converted to heat energy (Joule heating), and the fluid temperature rises as a result of Joule heating. The influence of Reynolds number on fluid temperature is shown in Figure 3D, it depicts a rising trend as Reynolds number increases. This can be attributed to increased frictional force, the Re values improve the thermal distribution of the fluid, hence a rise in fluid temperature.
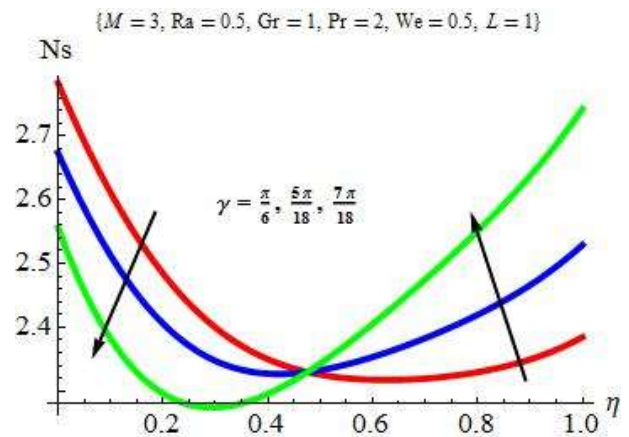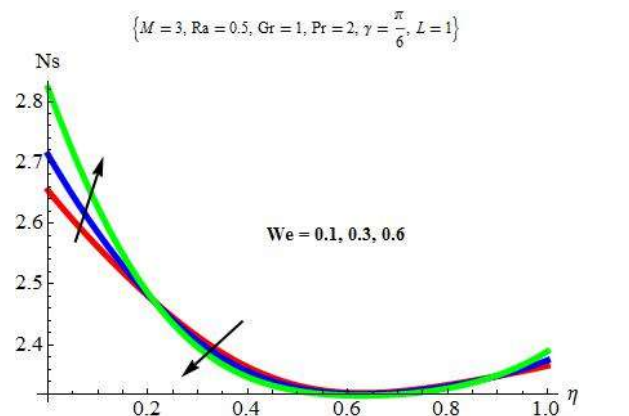

Fig. 4A: γ versus Entropy Generation

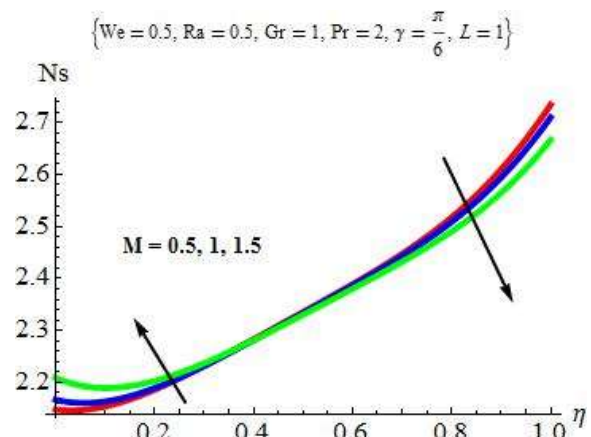

Fig. 4B: Weissenberg number versus Entropy Generation
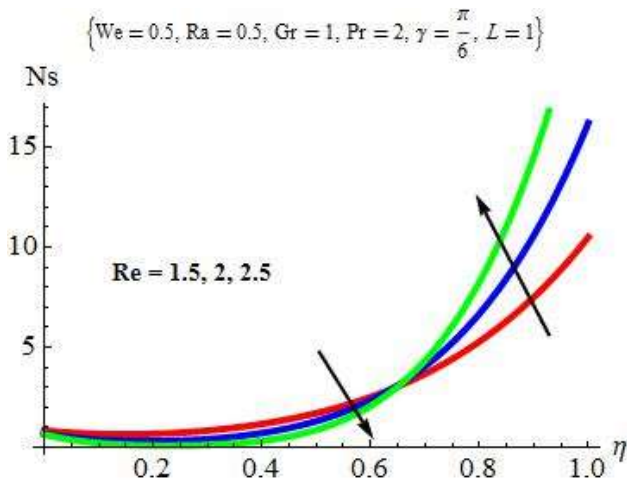

Fig. 4C: M versus Entropy Generation

$$\left\{We = 0.5, Ra = 0.5, Gr = 1, Pr = 2, \gamma = \frac{\pi}{6}, L = 1\right\}$$

Ns

Re = 1.5, 2, 2.5

Fig. 4D: Re versus Entropy Generation

$$\left\{M = 3, Ra = 0.5, Gr = 1, \gamma = \frac{\pi}{6}, We = 0.5, L = 1\right\}$$
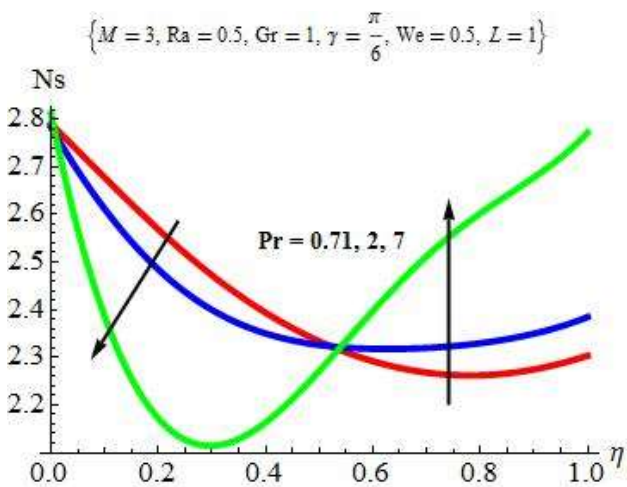
Ns

Pr = 0.71, 2, 7

Fig. 4E: Pr versus Entropy Generation

Figure 4 depicts the effects of various governing parameters on the entropy generation within the channel. As the angle of inclination parameter increases, Figure 4A shows a reduction in fluid entropy generation at the lower wall and an increase at the upper wall. The increase noticed at the upper wall is because higher fluid velocity increases the forces acting on the fluid flow, resulting in more entropy formation. The effect of Weissenberg number (We) on fluid entropy generation is presented in Figure 4B. As We increases, entropy generation enhances towards the channel's lower wall, with a marginal increase at the upper wall.This is due to the shear-thinning effect, which causes higher flow motion at the lower wall, as discussed in Figure 2B. Figures 4C and 4D present a falling trend in entropy generation at the lower wall with the reverse trend at the upper wall as magnetic field parameter and Reynolds number take higher values. With a high Reynolds number, disordered motion develops because the fluid moves more randomly as Re increases, and so the contribution of fluid

friction and heat transfer to entropy generation tends to increase. Figure 4E shows that entropy generation is significantly lowered at the lower channel but yields to a sharp rise at the upper channel as Prandtl number increases.
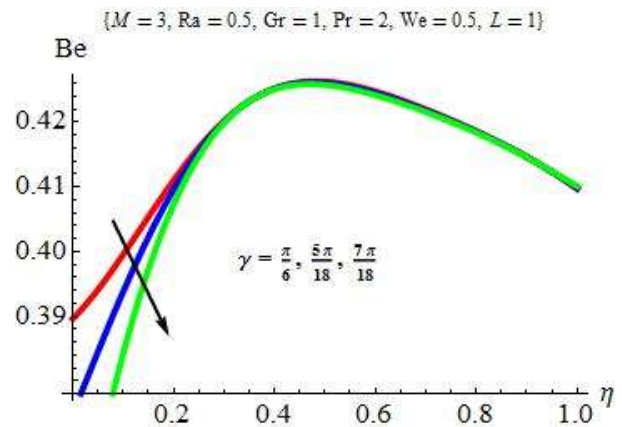
$$\{M = 3, Ra = 0.5, Gr = 1, Pr = 2, We = 0.5, L = 1\}$$

Be

$$\gamma = \frac{\pi}{6}, \frac{5\pi}{18}, \frac{7\pi}{18}$$

Fig. 5A: γ versus Bejan number

$$\left\{M = 3, Ra = 0.5, Gr = 1, Pr = 2, \gamma = \frac{\pi}{6}, L = 1\right\}$$

Be

We = 0.1, 0.3, 0.6

Fig. 5B: Weversus Bejan number

$$\left\{We = 0.5, Ra = 0.5, Gr = 1, Pr = 2, \gamma = \frac{\pi}{6}, L = 1\right\}$$

Be

M = 0.5, 1, 1.5

Fig. 5C: M versus Bejan number

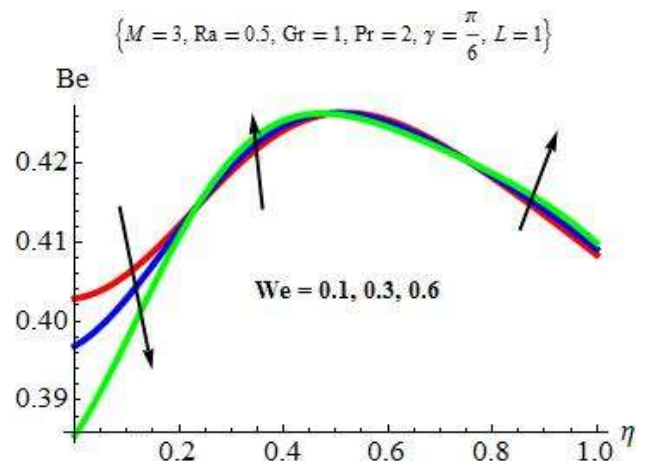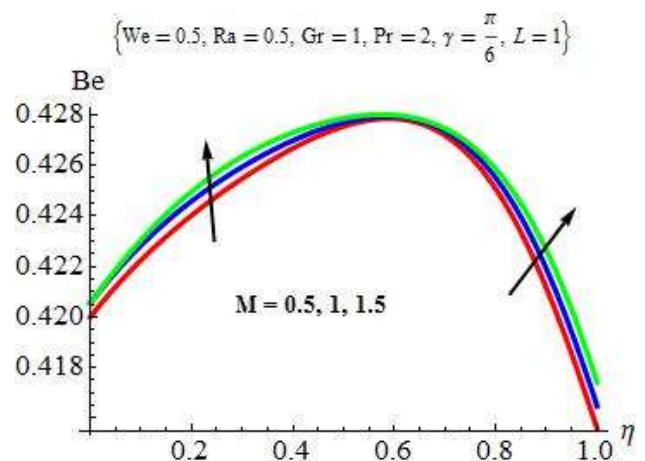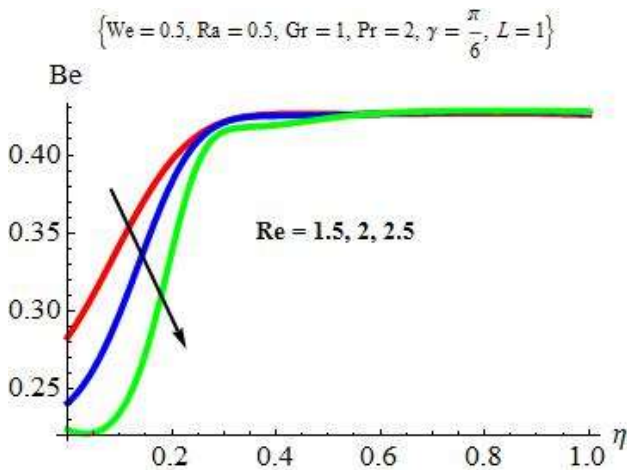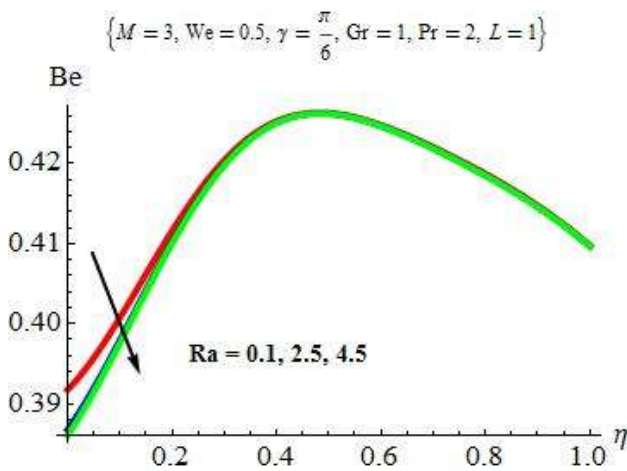Fig. 5D: Re versus Bejan number
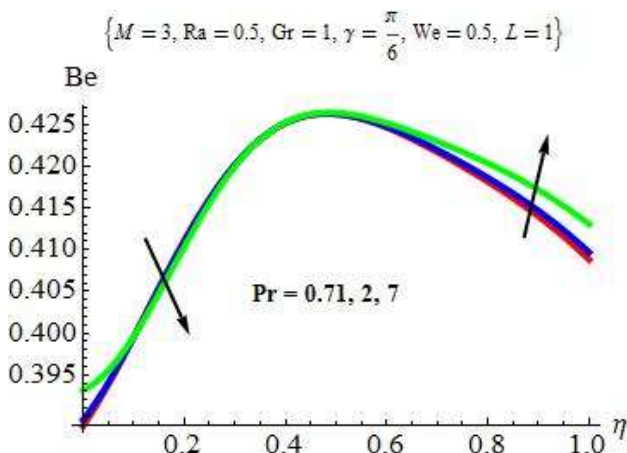

Fig. 5E: Ra versus Bejan number

Fig. 5F: Pr versus Bejan number

Figure 5 shows the reaction of the Bejan number to variations in the angle of inclination parameter, Weissenberg number, magnetic field parameter, Reynolds number, radiation parameter, and Prandtl number. In Figure 5A, it is obvious that fluid friction dominates entropy production because the Bejan number decreases at the lower wall as the angle of inclination parameter increases in value.

For Weissenberg number, fluid friction is effective in contributing to entropy formation at the lower wall, while heat transfer dominates at the middle and upper walls, as seen in Figure 5B. Heat transfer is the dominant contributor to entropy generation in Figure 5C because values of Bejan number grow with increasing magnetic field parameter throughout the entire channel. Figure 5D, on the other hand, shows a reversal of the pattern, since entropy generation decreases as Reynolds number rises. Finally, Figure 5E depicts that heat transfer dominates entropy generation as the radiation parameter increases. However, Figure 5F shows a reversal of the trend with a rise in the Prandtl number.

7 Conclusion

The heat irreversibility analysis of thermal radiation, Ohmic heating, and angle of inclination on Williamson fluid is investigated in this paper. The flow model equations obtained are non-dimensionalised and solved via homotopy perturbation technique. The entropy generation and Bejan number are analyzed using the results obtained for velocity and temperature profiles, and plots are presented to illustrate the flow characteristics for the velocity, temperature, entropy generation, and Bejan number. The main points are summarized as follows:

- The angle of inclination parameter and the radiation parameter increase fluid velocity, whereas the magnetic field parameter, Reynolds number, and Prandtl number reduce flow motion,
- The angle of inclination, magnetic parameter, Reynolds number, and radiation parameter all enhance fluid temperature,
- All of the factors, except the radiation parameter, promote entropy formation at the upper wall,
- For increasing values of the inclination parameter, Weissenberg number, Reynolds number, and radiation parameter, fluid friction dominates entropy generation, whereas the magnetic field parameter and Prandtl number reveal the dominance of heat irreversibility.

Future investigations can be directed to nonlinear thermal and internal heat generation as well as mass transfer rate.

References:

[1] R.V. Williamson, The flow of pseudoplastic materials, *Ind. Eng. Chem*. Vol. 21, No. 11, 1929, pp. 1108–1111. https://doi.org/10.1021/ie50239a035

[2] M. Ijaz Khan, F. Alzahrani, Activation energy and binary chemical reaction effect in nonlinear thermal radiative stagnation point flow of Walter-B nanoflid: numerical computations, *Int. J. Modern Physics B*, Vol. 34, No.13, 2020. https://doi.org/10.1142/S0217979220501325

[3] S. Nadeem, S.T. Hussain,C. Lee, Flow of a Williamson fluid over a stretching sheet.*Brazilian j. of Chem. Eng*., Vol. 30, No. 3, 2013, pp. 619-625. http://dx.doi.org/10.1590/S0104-66322013000300019

[4] T. Hayat, A. Shafiq, A. Alsaedi, Hydromagnetic boundary layer flow of Williamson fluid in the presence of thermal radiation and ohmic dissipation. *Alex. Eng. J*.Vol. 55, No. 3, 2016, pp. 2229-2240. http://dx.doi.org/10.1016%2Fj.aej.2016.06.004

[5] M.R. Krishnamurthy, B.C. Prasannakumara, B.J. Gireesha, R.S.R. Gorla, Effect of chemical reaction on MHD boundary layer flow and melting heat transfer of Williamson nanofluid in porous medium. *Eng. Sci. and Tech., an Int. J*., Vol. 19, No. 1, 2016,pp. 53-61. https://doi.org/10.1016/j.jestch.2015.06.010

[6] I. Dapra, G. Scarpi, Perturbation solution for pulsatile flow of a non-Newtonian Williamson fluid in a rock fracture. *Int. J. of Rock Mechs. and Mining Sci.*, Vol. 44, No. 2, 2007, pp. 271-278.http://dx.doi.org/10.1016/j.ijrmms.2006.07.003

[7] K. Vajravelu, S. Sreenadh, K. Rajanikanth, C. Lee, Peristaltic transport of a Williamson fluid in asymmetric channels with permeable walls. *Nonlinear Anal. Real World Appls*.,Vol. 13, No. 6, 2012, pp. 2804-2822. http://dx.doi.org/10.1016/j.nonrwa.2012.04.008

[8] J. Raza, F. Mebarek-Oudina, B. Mahanthesh, Magnetohydrodynamic flow of nano Williamson fluid generated by stretching plate with multiple slips, *Multidiscip. Model. Mater. Struct.*Vol. 15, No. 5, 2019,pp. 871–894. http://dx.doi.org/10.1108/MMMS-11-2018-0183

[9] C. Vasudev, U.R. Rao, M.V.S. Reddy, G.P. Rao, Peristaltic pumping of Williamson fluid through a porous medium in a horizontal channel with heat transfer. *American J. of Scientific and Ind. Research*,Vol. 1, No. 3, 2010, pp. 656-666. doi:10.5251/ajsir.2010.1.3.656.666

[10] S. Nadeem, S. Ashiq, M. Ali, Williamson fluid model for the peristaltic flow of chyme in small intestine. *Mathematical Problems in Eng*. 2012, https://doi.org/10.1155/2012/479087

[11] M.Y. Malik, T. Salahuddin, A. Hussain, S. Bilal, M. Awais, Homogeneous-heterogeneous reactions in Williamson fluid model over a stretching cylinder by using Keller box method. *AIP Adv.,*Vol. 5, No. 10, 2015. http://dx.doi.org/10.1063/1.4934937

[12] C. Vittal,M.C.K. Reddy,T. Vijayalaxmi,MHD Stagnation Point Flow and Heat Transfer of Williamson Fluid over Exponential Stretching Sheet Embedded in a Thermally Stratified Medium. *Global J. of Pure and Appl. Maths.*, Vol. 13, No. 6, 2017, pp. 2033-2056.

[13] M. Monica,J. Sucharitha, C.K. Kumar, Stagnation Point Flow of a Williamson Fluid over a Nonlinearly Stretching Sheet with Thermal Radiation, *American Chem. Sci. J*., Vol. 13, No. 4, 2016, pp. 1-8.https://doi.org/10.9734/ACSJ/2016/25144

[14] L. Nagaraja,M.S. Reddy, Heat transfer of non-Newtonian Williamson fluid flow past a circular cylinder with suction and injection. *Int. j. of Innovative Research in Sci. & Tech*., Vol. 6, No. 13, 2017, pp. 48-54.DOI: 10.17485/ijst/2017/v10i32/104601

[15] A.M. Siddiqui, S. Bhatti, M.A. Rana,M. Zahid, Blade coating analysis of a Williamson fluid. *Results in Phys*., Vol. 7, 2017, pp. 2845-2850. https://doi.org/10.1016/j.rinp.2017.07.076

[16] N.S. Shashikumar, Macha Madhu, S. Sindhu, B.J. Gireesha, NaikotiKishan Thermal analysis of MHD Williamson fluid flow through a microchannel, *International Communications in Heat and MassTransfer*,Vol. 127, 2021. https://doi.org/10.1016/j.icheatmasstransfer.2021.105582

[17] B.M.J. Rana, S.M. Arifuzzaman, Saiful Islam, Sk. Reza-E-Rabbi, Abdullah Al-Mamun, MalatiMazumder, Kanak Chandra Roy, Md. Shakhaoath Khan Swimming of microbes in blood flow of nano-bioconvective Williamson fluid, *Thermal Science and Engineering Progress*, Vol. 25, 2021.https://doi.org/10.1016/j.tsep.2021.101018

[18] B.M.J. Rana1, S.M. Arifuzzaman, Sk. Reza-E-Rabbi, S.F. Ahmed, Md. Shakhaoath Khan, Energy and Magnetic Flow Analysis of Williamson Micropolar Nanofluid through Stretching Sheet, *International Journal of Heat and Technology*, Vol. 37, No. 2, 2019, pp. 487-496. http://dx.doi.org/10.18280/ijht.370215

[19] W. G. Khalaf and S. K. Sastry, Effect of fluid viscosity on the Ohmic heating rate of solid-liquidmixtures, *J. Food Eng*. Vol. 27, No. 2, 1996, pp. 145-158. https://doi.org/10.1016/0260-8774(94)00090-5

[20] J. A. Rao, G. Vasumathi and J. Mounica, Joule heating and thermal radiation effects on MHD boundary layer flow of a nanofluid over an exponentially stretching sheet in a porous medium, *World J. Mech.*Vol. 5, No. 9, 2015,pp. 151-164. http://dx.doi.org/10.4236/wjm.2015.59016

[21] D. Prakash, P. Suriyakumar and Narsu Sivakumar and B. Rushi Kumar, Influence of viscous andOhmic heating on MHD flow of nanofluid over an inclined nonlinear stretching sheet embedded in a porous medium, *Int. J. Mech. Eng. Technol.*Vol. 9, No. 8, 2018, pp. 992-1001. http://iaeme.com/Home/issue/IJMET

[22] R. Tsai, K. H. Huang and J. S. Huang, The effects of variable viscosity and thermal conductivity onHeat transfer for hydromagnetic flow over a continuous moving porous plate with Ohmic heating, *Appl. Therm. Eng.*Vol. 29, No. 10, 2009, pp. 1921-1926. http://dx.doi.org/10.1016%2Fj.applthermaleng.2008.09.005

[23] B. Awasthi, Joule heating effect in presence of thermal radiation on MHD convective flow past overa vertical surface in a porous medium, *Int. J. Eng. Sci. Invent*. Vol. 6, No. 9, 2017, pp. 117-134. DOI: 10.5958/2320-3226.2019.00011.0

[24] T. Muhammad, T. Hayat, S. A. Shehzad and A. Alsaedi, Viscous dissipation and Joule heating effectsin MHD 3D flow with heat and mass fluxes, *Results Phys*. Vol. 8, 2018, pp. 365-371.https://doi.org/10.1016/j.rinp.2017.12.047

[25] K. S. Adegbie, D. J. Samuel and B. O. Ajayi, Ohmic heating of magnetohydrodynamic viscous flow over a continuous moving plate with viscous dissipation buoyancy and thermal radiation, *Defect Diffusion Forum*. Vol. 392: 2019, pp. 73-91. https://doi.org/10.4028/www.scientific.net/ddf.392.73

[26] E. Osalusi, J. Side and R. Harris, The effects of Ohmic heating and viscous dissipation on unsteadyMHD and slip flow over a porous rotating disk with variable properties in the presence of Hall andion-slip currents, *Int. Commun. Heat Mass Transf*. Vol. 34, Nos.9-10, 2007, pp. 1017-1029. https://doi.org/10.1016/j.icheatmasstransfer.2007.05.009

[27] B.S. Goud, M.M. Nandeppanavar, Ohmic heating and chemical reaction effect on MHD flow of micropolar fluid past a stretching surface, *Partial Differential Equations in Applied Mathematics*, Vol. 4, 2021 https://doi.org/10.1016/j.padiff.2021.100104

[28] Md. M. Hasan, Md. A. Samad and Md M. Hossain, Effects of Hall Current and Ohmic Heating onNon-Newtonian Fluid Flow in a Channel due to Peristaltic Wave, *Applied Mathematics-a Journal of Chinese Universities Series B*, Vol. 11, 2020,pp. 292-306. https://doi.org/10.4236/am.2020.114022

[29] B.J. Gireesha, K. Ganesh Kumar, M.R. Krishnamurthy, S. Manjunatha, N.G. Rudraswamy, Impact of Ohmic heating on MHD mixed convection flow of Casson fluid by considering Cross diffusion effect, *Nonlinear Engineering,*Vol. 8, No. 1, 2019, pp. 380-388. https://doi.org/10.1515/nleng-2017-0144

[30] D.J. Samuel and B.I. Olajuwon, Insight into the effects of thermal radiation and Ohmic heating onchemically reactive Maxwell fluid subject to Lorentz force and buoyancy force, *Journal of the Nigerian Mathematical Society*, Vol. 41, No. 1, 2022, pp. 27-48. https://ojs.ictp.it/jnms/index.php/jnms/article/view/767

[31] A. Bejan, *Entropy Generation through Heat and Fluid Flow*, Wiley, New York, 1982.

[32] A. Bejan, *Convection Heat Transfer*, Wiley, New York, 2004.

[33] A. Bejan, A study of entropy generation in fundamental convective heat transfer, *J. Heat Transf*. Vol. 101, 1979, pp. 718-725.

[34] A. Bejan, Second law analysis in heat transfer and thermal design, *Adv. Heat Tran*. Vol. 15, 1982, pp. 1-58.http://dx.doi.org/10.1016/S0065-2717(08)70172-2

[35] S. Saouli, S. Aïboud-Saouli, Second law analysis of laminar falling liquid film along an inclined heated plate, *Int. Commun. Heat Mass Transfer*.Vol. 31, 2004, pp. 879–886.

[36] M. Havzali, A. Arikoglu, G. Komurgoz, H.I. Keser, I. Ozkol, Analytical–numerical analysis of entropy generation for gravity-driven inclined channel flow with initial transition and entrance effects, *Phys. Scr*. Vol. 78, 2008. http://dx.doi.org/10.1088/0031-8949/78/04/045401

[37] M.S. Tshehla, The flow of a variable viscosity fluid down an inclined plane with a free surface, *Math. Probl. Eng*. 2013 http://dx.doi.org/10.1155/2013/754782

[38] A.I. Al-Ahmed, R.K. A.Z. Sahin, M.H. Arshad, Second law analysis of a gravity-driven liquid film flowing along an inclined plate subjected to constant wall temperature, *Int. J. Exergy*, Vol. 14, No. 2, 2014, pp. 156-178.

[39] S.O. Adesanya, S.O. Kareem, A.J. Falade, S.A. Arekete, Entropy generation analysis for a reactive couple stress fluid flow through a channel saturated with porous material. *Energy*Vol. 93, 2015, pp. 1239–1245. https://ideas.repec.org/a/eee/energy/v93y2015ip1p1239-1245.html

[40] S.O. Adesanya, O.D. Makinde, Thermodynamic analysis for a third grade fluid through a vertical channel with internal heat generation. *J. Hydrodyn*.,Vol. 27, 2, 2015, pp. 264–272.

[41] S.S.S. Sen, M. Das, R. Mahato, S. Shaw, Entropy analysis on nonlinear radiative MHD flow of Diamond-Co3O4/ethylene glycol hybrid nanoflid with catalytic effects, *International Communications in Heat and Mass Transfer*, Vol. 129, 2021.https://doi.org/10.1016/j.icheatmasstransfer.2021.105704

[42] S. Shaw, M.K. Nayak, A.S. Dogonchi, A. J. Chamkha, Y. Elmasry, R. Alsulami, Hydrothermal and entropy production analyses of magneto-cross nanoliquid under rectifid Fourier viewpoint: A robust approach to industrial applications, *Case Studies in Thermal Engineering*Vol. 26, 2021. https://doi.org/10.1016/j.csite.2021.100974

[43] M.K. Nayak, S. Shaw, M. Ijaz Khan, O.D. Makinde, Yu-Ming Chu, S.U. Khan, Interfacial layer and shape effects of modified Hamilton's Crosser model in entropy optimized Darcy-Forchheimer flow, *Alexandria Engineering Journal*, Vol. 60, 2021,pp. 4067–4083.https://doi.org/10.1016/j.aej.2021.02.010

[44] Opanuga AA, Agboola OO, Gbadeyan JA, Okagbue HI (2020) Entropy generation analysis of Hall current effect on MHD micropolar fluid flow with rotation effect, SN Applied Sciences. https://doi.org/10.1007/s42452-019-1783-7

[45] Opanuga AA, Gbadeyan JA, Agboola OO, Okagbue HI (2018) Effect of suction/injection on the entropy generation of third grade fluid with convective cooling. Defect and Diffusion Forum 384:465-474.

[46] Opanuga AA, Gbadeyan JA, Iyase SA (2017) Second law analysis of hydromagnetic couple stress fluid embedded in a non-Darcian porous medium. IAENG International Journal sof Applied Mathematics. 47(3):287-294

[47] J.H. He, A coupling method of a homotopy technique and a perturbation technique for non-linear problems, *International Journal of Non-Linear Mechanics*, Vol. 35, No. 1, 2000, pp. 37-43. https://doi.org/10.1016/S0020-7462(98)00085-7

[48] J.H. He, Homotopy perturbation technique, *Computer Methods in Applied Mechanics and Engineering*, Vol. 178, Nos. 3-4, 1999, pp. 257–262. http://dx.doi.org/10.1016/S0045-7825(99)00018-3

[49] J. H. He, Homotopy perturbation method: a new nonlinear analytical technique, *Applied Mathematics and Computation*, Vol. 135, No. 1, 2003, pp. 73–79.http://dx.doi.org/10.1016/S0096-3003(01)00312-5

[50] J.H. He, A simple perturbation approach to Blasius equation,*Applied Mathematics and Computation,*Vol. 140, Nos. 2-3, 2003, pp. 217–222.http://dx.doi.org/10.1016/S0096-3003(02)00189-3

[51] J. H. He, Application of homotopy perturbation method to nonlinear wave equations,*Chaos, Solitons and Fractals*, Vol. 26, No. 3, 2005, pp. 695–700. http://dx.doi.org/10.1016/j.chaos.2005.03.006

[52] J.H. He, Homotopy perturbation method for solving boundary value problems, *Physics Letters A,*Vol. 350, Nos. 1-2, 2006, pp. 87–88.http://dx.doi.org/10.1016/j.physleta.2005.10.005

[53] A. Belendez, C. Pascual, S. Gallego, M. Ortu, C. Neipp,Application of a modified He's homotopy perturbation method to obtain higher-order approximations of an $x^{1/3}$ force nonlinear oscillator, *Physics Letters A*, Vol. 371, Nos. 5-6, 2007, pp. 421–426. https://doi.org/10.1016/j.physleta.2007.06.042

[54] Z. Odibat and S. Momani, Modified homotopy perturbation method:Aapplication to quadratic Riccati differential equation of fractional order,Chaos, *Solitons and Fractals*, vol. 36, No. 1, pp. 167–174, 2008 http://dx.doi.org/10.1016/j.chaos.2006.06.041

[55] Z. M. Odibat, A new modifiation of the homotopy perturbation method for linear and nonlinear operators,*Applied Mathematics and Computation*, Vol. 189, No. 1, 2007, pp. 746–753. https://doi.org/10.1016/j.amc.2006.11.188

[56] George Oguntala, GbeminiyiSobamowo, Yinusa Ahmed and RaedAbd-Alhameed, Application of Approximate Analytical Technique Using the Homotopy Perturbation Method to Study the Inclination Effect on the Thermal Behavior of Porous Fin Heat Sink, *Math. Comput. Appl*., Vol. 23, No. 4, 2018. https://doi.org/10.3390/mca23040062

[57] O.D. Makinde 1 and A.S. Eegunjobi, Effects of Convective Heating on Entropy Generation Rate in aChannel with Permeable Walls, *Entropy*, Vol. 15, 2013, pp. 220-233. http://dx.doi.org/10.3390/e15010220

Contribution of Individual Authors to the Creation of a Scientific Article (Ghostwriting Policy)

Conception and design of the model by Opanuga and Sobamowo

non-dimensionalised the model was carried out by Ogunniyi,

Solution and analysis of the model was performed by Opanuga,

Typesetting and proofreading by Okagbueand

Interpretation of results by Sobamowo.

Abiodun Opanuga, Gbeminiyi Sobamowo,
Hilary Okagbue, Peter Ogunniyi

Appendix
Nomenclature

u, v Velocity components along x and y directions respectively,

v Kinematic viscosity,

k Thermal conductivity,

c_p Specific heat of the fluid at constant pressure,

ρ Fluid density,

g Acceleration due to gravity,

μ Dynamic viscosity,

T Temperature of the fluid,

θ Dimensionless temperature,

B_0^2 Magnetic field parameter,

γ Angle of inclination,

We Weissenberg number,

Re   Reynolds number,

M Magnetic parameter,

Pr   Prandtl number,

Ra Thermal radiation parameter,

Ec Eckert number,

Be Bejan number,

A Constant pressure gradient,

Gr Grashof number,

Γ Material fluid parameter,

h Channel width,

E_G Local volumetric entropy,

Ns Dimensionless entropy generation parameter,

q_r Radiative heat flux,

k^c Rosseland mean absorption coefficient,

σ^c Stefan-Boltzmann constant,

σ Electrical conductivity of the fluid,

β Coefficient of thermal expansion,

L Characteristic temperature ratio.